

# Plasma membrane aquaporins interact with the endoplasmic reticulum resident VAP27 proteins at ER–PM contact sites and endocytic structures

Ana Romina Fox<sup>1,2</sup> , Florencia Scochera<sup>2,3</sup>, Timothée Laloux<sup>1</sup>, Karolina Filik<sup>1</sup> , Hervé Degand<sup>1</sup>, Pierre Morsomme<sup>1</sup> , Karina Alleva<sup>2,3</sup>  and François Chaumont<sup>1</sup> 

<sup>1</sup>Louvain Institute of Biomolecular Science and Technology, UCLouvain, Louvain-la-Neuve 1348, Belgium; <sup>2</sup>Facultad de Farmacia y Bioquímica, Instituto de Química y Físicoquímica Biológica (IQIFIB), CONICET, Universidad de Buenos Aires, Buenos Aires 1113, Argentina; <sup>3</sup>Facultad de Farmacia y Bioquímica, Departamento de Fisicomatemática, Universidad de Buenos Aires, Buenos Aires 1113, Argentina

## Summary

Author for correspondence:  
François Chaumont  
Tel: +32 10 47 84 85  
Email: francois.chaumont@uclouvain.be

Received: 3 April 2020  
Accepted: 1 June 2020

*New Phytologist* (2020) **228**: 973–988  
doi: 10.1111/nph.16743

**Key words:** aquaporin, endocytosis, endoplasmic reticulum (ER), endoplasmic reticulum–plasma membrane (ER–PM) contact sites (EPCSs), plant vesicle-associated membrane protein (VAMP)-associated protein (VAP27), plasma membrane intrinsic protein (PIP).

- Plasma membrane (PM) intrinsic proteins (PIPs) are aquaporins facilitating the diffusion of water and small solutes. The functional importance of the PM organisation of PIPs in the interaction with other cellular structures is not completely understood.
- We performed a pull-down assay using maize (*Zea mays*) suspension cells expressing YFP-*ZmPIP2;5* and validated the protein interactions by yeast split-ubiquitin and bimolecular fluorescence complementation assays. We expressed interacting proteins tagged with fluorescent proteins in *Nicotiana benthamiana* leaves and performed water transport assays in oocytes. Finally, a phylogenetic analysis was conducted.
- The PM-located *ZmPIP2;5* physically interacts with the endoplasmic reticulum (ER) resident *ZmVAP27-1*. This interaction requires the *ZmVAP27-1* cytoplasmic major sperm domain. *ZmPIP2;5* and *ZmVAP27-1* localise in close vicinity in ER–PM contact sites (EPCSs) and endocytic structures upon exposure to salt stress conditions. This interaction enhances PM water permeability in oocytes. Similarly, the Arabidopsis *ZmVAP27-1* paralogue, *AtVAP27-1*, interacts with the *AtPIP2;7* aquaporin.
- Together, these data indicate that the PIP2–VAP27 interaction in EPCSs is evolutionarily conserved, and suggest that VAP27 might stabilise the aquaporins and guide their endocytosis in response to salt stress.

## Introduction

Plasma membrane (PM) intrinsic proteins (PIPs) are aquaporins that facilitate the diffusion of water and small solutes through lipid bilayers (Maurel *et al.*, 2015; Fox *et al.*, 2017). PIP main function is exerted at the PM, where different lateral channel diffusion patterns exist (Li *et al.*, 2011). Some channels move freely, whereas others localise in restricted lateral diffusion regions such as microdomains (Li *et al.*, 2011). Interestingly, other cellular structures in addition to the PM, such as the cell wall (Martiniere *et al.*, 2012) and actin filaments (Hosy *et al.*, 2015), are involved in PIP lateral diffusion restriction, which reflects PIP close interaction with other cellular structures. The functional importance of PIP PM organisation in interactions with proteins/lipids from other cellular structures is not completely understood, but the role of PIP microdomains in the regulation of exo/endocytosis was proposed (Takano *et al.*, 2017).

Interorganelle contacts through membrane contact sites are involved in the maintenance of phospholipid homeostasis and

trafficking events (Pérez-Sancho *et al.*, 2016). These contact types among organelles are not randomly established but follow patterns that change when cellular nutrient status is modified or the cytoskeleton disassembled (Valm *et al.*, 2017). Recently, it was shown that ER–PM contact sites (EPCSs) were enhanced by ionic stress (Lee *et al.*, 2019), which is especially relevant for plant cells. EPCS proteomes are not yet clearly established, but evidence points to the existence of different EPCS populations (Siao *et al.*, 2016; Stefano *et al.*, 2018). In recent years, plant vesicle-associated membrane protein (VAMP)-associated proteins (VAP27s) and synaptotagmins (SYTs) have been characterised as evolutionarily conserved ER tethers that maintain the ER membrane in close proximity to the PM without fusing them (Wang *et al.*, 2014, 2016; Pérez-Sancho *et al.*, 2015). Arabidopsis STY1 interacts with the SNARE SYP121 and is involved in endocytosis and endosome recycling to the PM (Lewis & Lazarowitz, 2010; Kim *et al.*, 2016). Also, plant VAP interaction with a specific phosphoinositide (PI) subset in clathrin-mediated endocytosis has been reported (Stefano *et al.*, 2018). Consistently, in ER–

endosome membrane contact sites from mammal cells, VAPs are necessary to downregulate specific PI endosome levels and to ensure correct actin filament deposition (Dong *et al.*, 2016). Markedly, PIP endocytosis and autophagic degradation occurs in a PI-dependent manner (Ueda *et al.*, 2016; Jurkiewicz *et al.*, 2020), and different PIP isoforms are highly expressed in cell elongation zones (Heinen *et al.*, 2009), regions where the EPCSs are abundant (McFarlane *et al.*, 2017). However, evidence for PIP presence at EPCSs has not been shown yet.

Complex posttranslational regulation of eukaryotic aquaporins is mediated by other proteins (Roche & Törnroth-Horsefield, 2017). For instance, hundreds of putative *AIP* interactors were found (Bellati *et al.*, 2016). PIP cytosolic domains (i.e. the N- and C-termini, loops B and D) are involved in the regulation of channel trafficking, degradation, and gating upon interaction with specific proteins (Lee *et al.*, 2009; Zelazny *et al.*, 2009; Wu *et al.*, 2013; Hachez *et al.*, 2014a; Grondin *et al.*, 2015; Li *et al.*, 2015; Afzal *et al.*, 2016; Bellati *et al.*, 2016). In the present work, we explored which are the main partners of maize (*Zea mays*) *ZmPIP2;5*, the most highly expressed PIP isoform in roots involved in radial water movement (Hachez *et al.*, 2006; Ding *et al.*, 2020). We found that *ZmPIP2;5* interacts with *VAP27s* inserted in the ER membrane, and that this interaction positively influences PM water permeability. We propose that *VAP27s* stabilise PIP2s at the PM and might guide their endocytosis in response to salt stress. This interaction seems to be conserved through land plant evolution.

## Materials and Methods

### Genetic constructs

Total RNA was extracted from 6-d-old maize Black Mexican Sweet (BMS) cells using the RNeasy Plant Mini Kit (Qiagen, Hilden, Germany) following the manufacturer's instructions. Total cDNA was synthesised from RNA (1 µg) in a 25-µl reaction volume using M-MLV Reverse Transcriptase (Promega, Madison, WI, USA) and the oligo(dT)15 primer. For the SUS assay, *ZmVAP27-1* and *ZmVAP27-2* cDNAs were PCR amplified from BMS cell total cDNA, and *ZmPIP2;5* cDNA, optimised for expression in yeast, was PCR amplified from pYeDP60u-*ZmPIP2;5*<sup>OPT</sup> (Bienert *et al.*, 2014) using the corresponding att1B and att2B primers (Supporting Information Table S1). The PCR products were cloned with the Gateway<sup>®</sup> system (Invitrogen, Waltham, MA, USA) into the pDONR221P1P2 entry vector before their integration into the SUS destination vectors. pMetYC-DEST and pNX35-DEST (Grefen *et al.*, 2009) were used to produce the Met-repressible bait construct *ZmPIP2;5-Cub-PLV* and the prey constructs *NubG-ZmVAP27-1* or *NubG-ZmVAP27-2*, respectively. The NubWT control fragment was obtained from the pNubWT-Xgate vector (Grefen *et al.*, 2009).

To carry out bimolecular fluorescence complementation (BiFC) and localisation assays the cDNAs were cloned with the Gateway<sup>®</sup> system (Invitrogen). Briefly, *ZmPIP2;5* and *ZmVAP27-1* were PCR amplified using the corresponding attB1 and attB4 primers

and cloned into the pDONR221P1P4 entry vector. *ZmSYP121*, *ZmVAP27-1*, *ZmVAP27-2*, *AtVAP27-1*, *NpPMA2* and the deleted *ZmVAP27-1* versions ( $\Delta$ MSD and  $\Delta$ TMD) were PCR amplified using the corresponding attB3 and attB2 primers. For the  $\Delta$ CCD mutant genetic construct, two PCR fragments obtained with the attB3AtVAP27-1NFw/RvVAP11deltaCCD and attB2AtVAP27-1NRv/FwVAP11deltaCCD primer pairs were assembled in a second PCR with the attB3 and attB2 primers. All these PCR fragments were cloned into the pDONR221P3P2 entry vector. Details of the plasmid *pDONR221P1P4-AtPIP2;7* were previously published by our laboratory (Hachez *et al.*, 2014a). The vector Gateway<sup>®</sup> cassettes were transferred to the pBIFCt-2in1-NN destination vector (Grefen & Blatt, 2012) and/or the pFRETv-2in1-NN (Hecker *et al.*, 2015).

For the oocyte swelling assays, the pT7Ts-derived vector containing the T7 RNA polymerase promoter and carrying the 5' and 3' translated regions of the *Xenopus laevis*  $\beta$ -globin gene (Gorgoni *et al.*, 1995) was modified to add new cloning sites. Briefly, overlapping oligos with the recognition sites for *NotI*, *XhoI*, and *SacI* (Table S1) were annealed and cloned into the vector previously linearised using the *BglI* and *SpeI* enzymes. The *ZmPIP2;5* and *ZmVAP27-1* cDNAs were PCR amplified from BiFC vectors using specific primers to add restriction enzyme sites (Table S1). *ZmPIP2;5* was cloned into the *BglI* and *SpeI* sites, and *ZmVAP27-1* was cloned into the *SacI* and *SpeI* sites. All cloned products were checked by sequencing.

### Transfection of maize BMS cells

BMS cells were cultivated in the dark with constant shaking at 90 rpm and 25°C, in BMS medium (50 ml) (4.4 g l<sup>-1</sup> Murashige and Skoog basal salts with minimal organics; M6899, Sigma Aldrich, St. Louis, MO, USA), 30 g l<sup>-1</sup> sucrose, 3 mg l<sup>-1</sup> 2,4-dichlorophenoxyacetic acid (D8407, Sigma Aldrich), and 0.2 g l<sup>-1</sup> of L-Asn (A4284, Sigma Aldrich), pH 5.8). The cells were subcultured every 14 d at a 1:10 ratio with fresh BMS medium at room temperature.

Stable transfected BMS cells were obtained using the PDS-1000/He Biolistic particle bombardment delivery system (Bio-Rad, Hercules, CA, USA). Briefly, *pCAMBIA35Su:YFP-PIP2;5* (Chevalier *et al.*, 2014) and *pCAMBIA35Su:YFP* (Ding *et al.*, 2020) DNAs were precipitated onto 0.6 µm gold particles. These DNA-coated particles were used to bombard 9-d-old BMS cells spread over Whatman filters on top of BMS medium-agar plates. After 3 d the filters were transferred to selective BMS medium plates (kanamycin 100 µg ml<sup>-1</sup> for *pCAMBIA35Su:YFP-PIP2;5* and Bialaphos 3 µg ml<sup>-1</sup> for *pCAMBIA35Su:YFP*). Every 15 d the filters were transferred to fresh plates. Fluorescent calli were selected after 4–6 wk.

### Protoplast swelling assay

BMS protoplast isolation was performed as described previously (Moshelion *et al.*, 2004). Briefly, protoplasts were isolated from 2 ml of 8-d-old BMS cell suspensions. The cells were left to sediment and the BMS medium was replaced with cell wall digestion

solution (1 ml) (1.5% w/v cellulase Y-C; Kyowa Chemical Products, Japan), 0.3% w/v Macerozyme R-10 (Duchefa Biochemie, Haarlem, the Netherlands) in isotonic solution (to be described later). The cells were placed on a rotary shaker (90 rpm) for 2 h 30 min at 26°C. Then, the cells were passed through a nylon filter (20 µm pore size) and washed two times with isotonic solution. The protoplast swelling experiments were performed as described previously (Moshelion *et al.*, 2004). The isotonic and hypotonic solutions (10 mM KCl, 1 mM CaCl<sub>2</sub>, 8 mM MES, pH 5.75) were adjusted with sorbitol to 300–330 and 150–160 mOsm, respectively. The Advanced Instruments 3300 Micro-Osmometer (Advanced Instruments, MA, USA) served for all osmolarity measurements.

#### Plant microsomal fraction preparation, immunoprecipitation and LC-MS assays

BMS cells were grown in 200 ml cultures and harvested after 7 d. The cells were washed with ice-cold homogenisation buffer (250 mM sorbitol, 50 mM Tris-HCl pH 8, 2 mM 2-[2-[bis(carboxymethyl)amino]ethyl-(carboxymethyl)amino]acetic acid (EDTA), 10 mM dithiothreitol (DTT), 1 mM phenylmethylsulphonyl fluoride (PMSF), and 2 µg ml<sup>-1</sup> each of leupeptin, pepstatin, aprotinin, antipain and chymostatin) and ground with glass beads. Cell debris was removed by centrifugation for 5 min at 3500 g. The supernatant was then centrifuged for 30 min at 100 000 g. Finally, the pellet corresponding to the microsomal fraction was suspended in resuspension buffer (250 mM sucrose, 20 mM HEPES pH 7.4, 10 mM KCl, 1.5 mM MgCl<sub>2</sub>, 1 mM EDTA, 1 mM 2-[2-[2-[bis(carboxymethyl)amino]ethoxy]ethoxy]ethyl-(carboxymethyl)amino]acetic acid (EGTA), 10 mM DTT, 1 mM PMSF, and 2 µg ml<sup>-1</sup> each of leupeptin, pepstatin, aprotinin, antipain and chymostatin). Proteins were quantified by the Bradford assay (Bradford, 1976) and adjusted to 3 mg ml<sup>-1</sup> and 1% w/v octyl-β-D-glucopyranoside. Protein extracts (15 mg) were mixed with 30 µl agarose beads (Chromotek, Planegg, Germany) and incubated in a rotor wheel for 1 h at 4°C. Then, the beads were pelleted by centrifugation at 2000 g for 10 s and the supernatant was incubated with 30 µl Chromotek GFP-Trap<sup>®</sup> agarose beads in a rotor wheel at 4°C overnight (ON). The beads were washed five times with 700 µl resuspension buffer supplemented with 300 mM NaCl. Bound proteins were eluted from the beads by adding 20 µl Laemmli buffer and incubating for 15 min at 65°C. This step was repeated twice. ZmPIP2;5 immunoprecipitation was confirmed in aliquots (2 µl) by immunoblot. The remaining samples were electrophoresed by SDS-PAGE just to stack the proteins that were in-gel digested with trypsin, and peptides recovered for the nano-ultra-high performance liquid chromatography coupled with electrospray ionisation-quadrupole-time of flight-mass spectrometry (nano-ULPC-ESI-QTOF-MS) analysis at the MASSPROT facility (UCLouvain, detailed protocol in Methods S1). For each sample, three technical replicates were run in the nano-ULPC-ESI-QTOF-MS. PROGENESIS QI (v.2.0, Nonlinear Dynamics) was used to analyse the spectrometry data. The runs were normalised to YFP levels. For peptide identification the maize

UP000007305 reference proteome was used (UniProt). Detailed information of the ions to peptides and peptides to proteins association is listed in Table S2. Progenesis QI software is not prepared to handle technical and biological replicates in statistical analysis. Therefore, to score the differential abundance of proteins between YFP-ZmPIP2;5 and YFP samples including technical replicates, the online freely available RepExplore software (Glaab & Schneider, 2015) was used. In this software the variance across technical replicates was included in the analysis using a Bayesian approach named probability of positive log ratio (PPLR) statistic (Glaab & Schneider, 2015).

#### Split-ubiquitin assays (SUS)

The haploid yeast strain THY.AP4 was cotransformed by electroporation with the Nub and Cub constructs of interest. Yeast colonies coexpressing the bait and prey constructs were recovered 48 h after transfer to selective medium (CSM, -Leu<sup>-</sup>, Trp<sup>-</sup>) (Grefen *et al.*, 2009). Growth assays were performed as detailed in Hachez *et al.* (2014a). Yeast coexpressing the Met-repressible bait construct ZmPIP2;5-Cub-PLV and the prey constructs NubG-ZmVAP27-1, NubG-ZmVAP27-2, NubG (negative control), or NubWT (positive control) were grown on selective medium. The next day, a dilution series (OD<sub>600</sub> nm 0.5, 0.05, and 0.005) of the cultures was dropped onto interaction-selective (CSM, -Leu<sup>-</sup>, Trp<sup>-</sup>, Ade<sup>-</sup>, His<sup>-</sup>, Met<sup>-</sup>) medium containing 100 µM methionine to repress bait expression. Control plates without methionine serve to verify that an equal yeast amount had been dropped. Yeast growth was recorded after incubation for 48 h at 30°C. Protein expression was verified via immunoblotting using a rat monoclonal antibody against the haemagglutinin (HA) tag (Roche, Mannheim, Germany) and a rabbit polyclonal antibody against VP16 (Abcam, Cambridge, UK), as previously described (Grefen *et al.*, 2009). Protein loading on a PVDF membrane was revealed by Coomassie R250 staining (Goldman *et al.*, 2016).

#### Confocal microscopy

A Zeiss LSM710 confocal microscope equipped with a spectral detector module (Carl Zeiss, Oberkochen, Germany) was used for confocal image acquisition. Imaging of BMS cells transformed with YFP-ZmPIP2;5 was achieved with a C-Apochromat ×40/1.20 water-immersion objective. The mYFP molecule was excited with the 514-nm laser lines. Emitted light was collected through a dichroic mirror on detector 520–560 nm. The cell PM was stained with FM4-64 dye (16 µM, Invitrogen). This dye was excited at 514 nm and detected from 600 to 760 nm.

The BiFC and localisation assays were performed in tobacco (*N. benthamiana*) epidermal cells transformed by *Agrobacterium tumefaciens* infiltration (Batoko *et al.*, 2000). Samples were analysed 3 d after infiltration. For fluorophore excitation and emission, the following laser settings were used: for mRFP1 excitation 561 nm and emission 560 to 615 nm, for mYFP excitation at 514 nm and emission 522 to 553 nm, for mTRQ2 excitation 445 nm and emission 463 to 520 nm, for mVenus excitation



514 nm and emission 520 to 574 nm. The BiFC analysis was performed using a  $\times 40/0.75$  water-immersion objective. Images were taken with standardised excitation intensities and photomultiplier gains. Relative fluorescence was analysed using the ZEN 2 Profile module (blue edn, Carl Zeiss). Five lines of five to six  $\mu\text{m}$  length were drawn through the PM of one cell. The fluorescence intensity of each line for each fluorophore was obtained. Then, the mYFP to mRFP1 fluorescence ratio of each line was calculated and averaged for that cell. The neighbour cells were not used to measure the fluorescence intensity to avoid including twice the values of a single cell. When specified, the Airyscan module (Carl Zeiss) and Plan-Apochromat  $\times 63/1.40$  oil immersion objective were used.

### *In vitro* RNA synthesis and oocyte water transport assays

The capped cRNA encoding for *ZmPIP2;5* was synthesised *in vitro* using the mMESSAGE mMACHINET7 High Yield Capped RNA Transcription Kit (Ambion, Austin, TX, USA), and the capped *ZmVAP27-1* cRNA was synthesised with the mMESSAGE mMACHINE T7 High Yield Capped RNA ULTRA Transcription Kit (Ambion), as described previously (Jozefkiewicz *et al.*, 2013). The synthesised products were resuspended in RNase-free water. cRNA integrity was checked on agarose gel and quantified in a NanoDrop<sup>TM</sup> 2000 spectrophotometer (Thermo Fisher Scientific).

Defolliculated *Xenopus laevis* oocytes (stages V–VI) were microinjected with cRNAs and incubated in ND96 buffer (96 mM NaCl, 2 mM KCl, 1 mM MgCl<sub>2</sub>, 1.8 mM CaCl<sub>2</sub>, and 5 mM HEPES pH 7.5; *c.* 200 mOsmol kg<sup>-1</sup> H<sub>2</sub>O) for 3 d at 18°C. The osmotic water permeability coefficient ( $P_f$ ) of oocytes injected or noninjected (NI) with cRNA was determined by measuring the oocyte swelling rate in response to ND96 buffer diluted five-fold with distilled water, as explained previously (Fortuna *et al.*, 2019). For pH inhibition experiments, the oocyte internal proton concentration was modified as explained previously (Bellati *et al.*, 2010), and the swelling response was induced by transferring the oocytes to an incubation solution diluted five-fold with distilled water. Briefly, oocytes were preincubated in solutions of different pH (MES for the 5.8 to 6.7 pH interval and HEPES for the 7.0–7.5 pH interval) containing 50 mM sodium acetate, 20 mM MES or HEPES, and supplemented with 1 M mannitol to adjust the osmolarity to *c.* 200 mOsmol kg<sup>-1</sup> H<sub>2</sub>O. To calculate the final internal pH in oocytes treated with acetate buffers, we used the calibration curve performed by Bellati *et al.* (2010). Noninjected oocytes, preincubated in a pH 7.5 solution for pH experiments, were used as negative controls. All osmolarities were measured in a vapour pressure osmometer (5600C; Wescor Inc., Logan, UT, USA).

### Bioinformatics analysis of *ZmVAP* proteins

Protein domains were identified with the Simple Modular Architecture Research Tool, SMART (Schultz *et al.*, 1998). Maize proteins containing a major sperm domain (MSD) domain were found in the B73 reference genome (RefGen\_v4) via a

BLAST search with *ZmVAP27-1* MSD, and also were found in the SMART database. *ZmVAP27* homologous gene families were identified in the Monocots PLAZA 4.0 platform (Van Bel *et al.*, 2018). For the phylogenetic tree, to obtain a harmonic representation of the different plant species, the protein sequences were retrieved from the family HOM04000421 (Monocots database), Dicots PLAZA 4.0, and Gymno PLAZA 1.0. Multiple sequence alignments (MSA) were assembled in the GUIDANCE2 server (Sela *et al.*, 2015) using the MAFFT (FFT-NS-100) algorithm. Unreliable sequences below a 0.60 confidence score were removed and the alignment redone. The sequences were trimmed with TRIMAL (Capella-Gutierrez *et al.*, 2009) removing unreliable columns below a 0.80 confidence score conserving 35% of the sequence. The best-fit model was found using MODELFINDER (Kalyaanamoorthy *et al.*, 2017) implemented in the IQ-TREE (v.1.10) Phylogenomic software. Branch support was calculated with the ultrafast bootstrap (Hoang *et al.*, 2018) and the SH-aLRT branch test (Guindon *et al.*, 2010). The best-fit model was JTT+F+R7. Trees were edited using the Interactive Tree of Life tool (Letunic & Bork, 2016). *ZmVAP* transcriptomic data were obtained and analysed using the GENEVESTIGATOR<sup>®</sup> v.4 platform (<https://genevestigator.com>) (Zimmermann *et al.*, 2004).

## Results

### Identification of *ZmPIP2;5* interactors associated with the cytoskeleton

We previously reported that the *ZmPIP2;5* physical interaction with the syntaxin SYP121 regulates its subcellular trafficking and water transport activity (Besserer *et al.*, 2012). To identify other *ZmPIP2;5* partners we designed a pull-down assay using BMS suspension cells. We generated transgenic lines that overexpressed YFP-*ZmPIP2;5* under the control of the 35S promoter and selected lines with high and stable protein expression levels. Confocal microscopy analysis showed that YFP-*ZmPIP2;5* was localised in the PM (Fig. 1a). We then determined the cell membrane  $P_f$  by protoplast swelling assays and observed that the  $P_f$  was greater in the *ZmPIP2;5* overexpression cells compared with wild-type cells (Fig. 1b), demonstrating that YFP-*ZmPIP2;5* was a functional water channel in these cells. We used this YFP-*ZmPIP2;5* overexpression cell line and a cell line overexpressing YFP (negative control) to perform a pull-down assay. With a *P*-like value  $< 0.05$  and fold change (FC)  $> 2$ , 138 proteins were defined as putative *ZmPIP2;5* interactors (Table S3). Then, we created a shorter interest list, which also included some proteins with a FC  $> 1.5$  (Table 1).

A cellulose synthase subunit (CESA) was pulled-down with *ZmPIP2;5*, similarly to that reported in a previous pull-down assay with *AtPIP2;1* (Bellati *et al.*, 2016). Interestingly, the CESA complex is one of the few identified mediators of the interaction between the PM and cortical microtubules (Krtková *et al.*, 2016), the latter guiding cellulose deposition (Paredes *et al.*, 2006). Then, we hypothesised that PIPs may also interact with the cytoskeleton, and that this interaction may underlie specific events regulating PIP function in cell water and/or solute

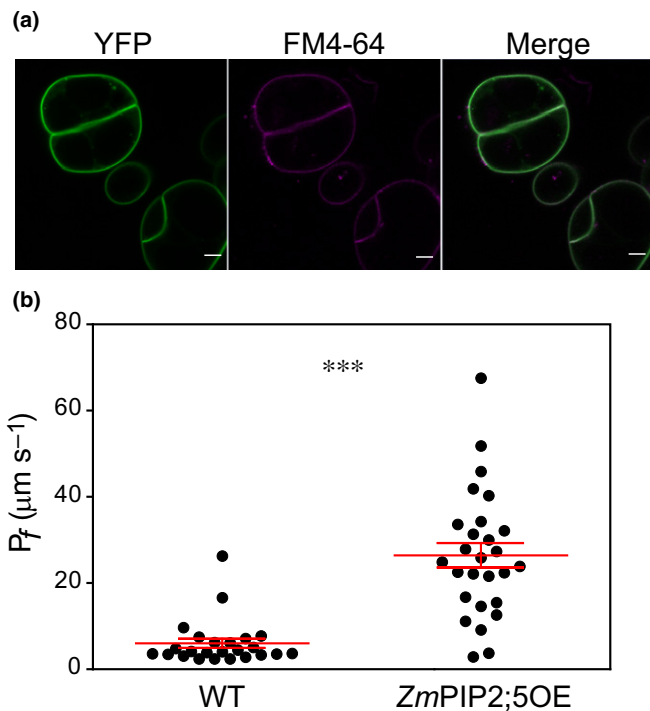


**Fig. 1** Localisation and activity of YFP-*ZmPIP2;5* expressed in Black Mexican Sweet (BMS) cells. (a) Confocal images of maize BMS cells stably transformed with the *35S::YFP-ZmPIP2;5* construct. A clear colocalisation of the YFP (green) and the plasma membrane dye FM4-64 (magenta) was observed. Bars, 10  $\mu\text{m}$ . (b) Water permeability coefficient ( $P_f$ ) values of nontransformed BMS cells (wild-type (WT)) and cells expressing YFP-*ZmPIP2;5* (*ZmPIP2;5OE*). For each scatter plot the lines indicate the mean  $\pm$  SE. An unpaired *t*-test was used to test the statistical difference between lines (\*\*\*,  $P < 0.001$ ).

homeostasis. In support of this hypothesis: (1) we observed the pull-down of proteins involved in PM–cytoskeleton association together with *ZmPIP2;5* (Table 1); (2) in a previous pull-down assay using *ZmPIP2;6* as bait, we identified kinesin, dynamin, actin, and tubulin as putative interactors (Hachez *et al.*, 2014a; Table S4); and (3) the reported *AtPIP2;1* pull-down assay also identified several dynamin and tubulin isoforms as interactors (Bellati *et al.*, 2016; Table S4). Markedly, we also identified two members of the plant-specific Networked (NET) actin-binding proteins superfamily (Deeks *et al.*, 2012), and two VAPs, *ZmVAP27-1* and *ZmVAP27-2*. VAPs and NETs, together with the cytoskeleton, are involved in EPCS organisation (Wang *et al.*, 2014). This evidence points to an association of the PM-localised *ZmPIP2;5* with the cortical cytoskeleton and ER, possibly through an interaction with *ZmVAP27-1* and *ZmVAP27-2*. Therefore, we decided to investigate the interaction between PIPs and VAP27s and its functional implications.

### *ZmPIP2;5* interacts with *ZmVAP27* proteins

To confirm the *ZmPIP2;5* interaction with *ZmVAP27-1* and *ZmVAP27-2*, we performed a yeast SUS. The cDNAs of *ZmVAP27-1* and *ZmVAP27-2* were cloned using BMS cell total RNA as a template. *ZmVAP27s* were N-terminal tagged with

NubG (prey) and *ZmPIP2;5* was C-terminal tagged with Cub-PLV (bait). NubG and NubWT fragments served as negative and positive controls of the Nub–Cub interaction, respectively (Grefen *et al.*, 2009). The specificity in the interaction was observed by reducing bait protein expression with methionine, which inhibited the *met25* promoter. Yeast growth was observed when *ZmPIP2;5*-Cub-PLV was expressed with both VAP27 proteins or with the positive NubWT control, whereas it was not observed for the negative control (Fig. 2a), indicating that *ZmPIP2;5* is able to physically interact with *ZmVAP27-1* or *ZmVAP27-2*. Bait and prey protein expression in the transformed yeast was confirmed by immunoblots (Fig. 2b).

Additionally, the physical interaction between *ZmPIP2;5* and *ZmVAP27s* was validated by a BiFC assay using the *pBiFCt-2in1* vector (Grefen & Blatt, 2012). This vector carries each protein of interest in frame with half of the YFP protein (YFPn and YFPc) and a soluble monomeric red fluorescent protein (mRFP1) as an internal transformation and expression control. *ZmSYP121* and *NpPMA2* were used as the positive and negative *ZmPIP2;5* interaction controls, respectively (Besserer *et al.*, 2012). The constructs were agro-infiltrated in *N. benthamiana* leaves and the fluorescence was observed by confocal microscopy after 3 d. For both the YFPn-*ZmPIP2;5*/YFPc-*ZmVAP27-1* and YFPn-*ZmPIP2;5*/YFPc-*ZmVAP27-2* pairs, a YFP fluorescent signal was detected with a particular bright dot pattern (insets Fig. 2c). As expected, a YFP fluorescent signal was also observed when YFPn-*ZmPIP2;5* was co-expressed with YFPc-*ZmSYP121*, whereas no signal was observed when YFPn-*ZmPIP2;5* was co-expressed with YFPc-*NpPMA2* (Fig. 2c). Additionally, we tested the specificity of the interaction between *ZmVAP27s* and *ZmPIP2;5* by analysing the YFPn-*ZmVAP27-1*/YFPc-*NpPMA2* pair, and did not detect any YFP signal, indicating that *ZmVAP27-1* is not broadly interacting with all PM proteins (Fig. S1). Altogether, the assays in the yeast heterologous system and in plant cells confirmed the pull-down data showing that *ZmVAP27-1* and *ZmVAP27-2* interacted with *ZmPIP2;5*.

### The MSD of VAP27s is required for PIP2–VAP27 interaction

Both *ZmVAP27-1* and *ZmVAP27-2* present the three characteristic VAP protein domains (Wang *et al.*, 2016): the cytoplasmic MSD, the coiled-coil domain (CCD), and the transmembrane domain (TMD) that anchors the protein to the ER (Fig. 3a). To determine which domain is involved in the interaction with *ZmPIP2;5*, we generated *ZmVAP27-1* mutants and tested their physical interaction with *ZmPIP2;5* by means of BiFC assays. Ratiometric fluorescence quantification resulted in a significant increase in the YFP/RFP ratio when the MSD was present in *ZmVAP27-1* (i.e. for the pairs YFPn-*ZmPIP2;5*/YFPc-*ZmVAP27-1*, YFPn-*ZmPIP2;5*/YFPc-*ZmVAP27-1* $\Delta$ TMD, and YFPn-*ZmPIP2;5*/YFPc-*ZmVAP27-1* $\Delta$ CCD), whereas the YFP/RFP ratio of the cells expressing YFPn-*ZmPIP2;5*/YFPc-*ZmVAP27-1* $\Delta$ MSD was not significantly different from the negative control (Fig. 3b; representative confocal images in Fig. S2a). The expression of *ZmVAP27-1* $\Delta$ MSD was confirmed by

**Table 1** Potential *ZmPIP2;5* interacting proteins.

Identifier	Description	P-like value	eBayes adj. P-value	Peptide count	Unique peptides	FC
Plasma membrane proteins						
Zm00001d017526	Aquaporin PIP1-2	1.6E-06	1.01E-04	9	2	8.3
Zm00001d017526	Aquaporin PIP1-3/PIP1-4	0.0E+00	2.61E-05	10	3	17.2
Zm00001d019565	Aquaporin PIP2-6	4.2E-10	1.48E-04	7	3	7.4
Zm00001d008178	ABC transporter B family member 21	5.2E-08	2.01E-03	29	7	2.1
Zm00001d013254	ABC transporter B family member 27	8.7E-09	2.36E-04	9	3	3.3
Zm00001d043766	ABC transporter B family member 9	1.8E-08	1.80E-03	5	2	2.2
Zm00001d048823	Monosaccharide-sensing protein 2	6.9E-03	8.27E-05	2	2	26.2
Zm00001d029762	Hexose transporter	1.5E-03	1.74E-02	4	3	1.6
Zm00001d005451	<b>Cellulose synthase A5</b>	3.3E-02	2.00E-02	10	3	1.7
Proteins involved in trafficking						
Zm00001d047468	<b>Aberrant pollen transmission1</b>	0.0E+00	1.18E-05	23	7	21.1
Zm00001d037842	B-cell receptor-associated 31-like	1.4E-04	4.70E-03	7	6	2.4
Zm00001d025817	<b>CLIP-associated protein (CLASP)</b>	8.6E-05	2.65E-03	12	4	2.1
Zm00001d014526	EH domain-containing protein 1	5.0E-07	1.95E-03	26	2	2.4
Zm00001d015102	Golgi SNAP receptor complex member 1	4.3E-03	2.27E-02	5	2	5.2
Zm00001d035041	Phospholipase SGR2	5.1E-03	4.82E-03	4	2	3.0
Zm00001d014159	<b>Protein Networked 1A</b>	2.0E-03	2.45E-03	5	2	2.3
Zm00001d014616	Transducin family protein/ WD-40 repeat family protein	0.0E+00	2.86E-06	2	2	46.2
Zm00001d042180	<b>Vesicle-associated protein 27-2</b>	1.4E-10	8.21E-03	4	2	6.5
Zm00001d025939	<b>Vesicle-associated protein 27-1</b>	2.6E-02	2.65E-03	3	3	2.3
Zm00001d038808	Vesicle-fusing ATPase	8.7E-09	2.80E-03	35	3	2.2
Zm00001d041443	<b>Protein Networked 1A</b>	8.3E-04	6.60E-03	10	2	1.8
Zm00001d021551	Ras-related protein RABH1b	2.3E-04	1.68E-02	16	7	1.7

Proteins in bold are involved in plasma membrane (PM)–cytoskeleton organisation (Pietra *et al.*, 2013; Paredes *et al.*, 2006; Deeks *et al.*, 2012; Wang *et al.*, 2014; Kirik *et al.*, 2007).

P-like value, transformation of the probability of positive log ratio (PPLR) into a P-like significance score; eBayes, empirical Bayes moderated *t*-statistic; FC, fold change.

confocal microscopy in tobacco leaves transiently expressing mTRQ2 tagged protein (Fig. S2b). Altogether, these data suggest that the VAP27 MSD domain is required for their interaction with *ZmPIP2;5*.

#### PIP2 C-terminal domain is not required for PIP2–VAP27 interaction

Most of the reported VAP interactors are cytoplasmic proteins with a binding motif of two phenylalanines in an acidic tract (FFAT) or a FFAT-like motif (Murphy & Levine, 2016). Using a mammal and yeast VAP interactome, an algorithm to predict VAP binding motifs was proposed (Murphy & Levine, 2016). We tested *ZmPIP2;5* cytoplasmic domains with that algorithm and found no putative interaction motifs within these sequences. However, this algorithm also predicted a weak interaction of the mammalian potassium channel Kv2.1, which is known to interact with VAP proteins through a noncanonical C-terminal domain binding motif that is rich in serine residues (Johnson *et al.*, 2018). As the *ZmPIP2;5* C-terminus is also serine rich, we tested whether this domain was required for the interaction with *ZmVAP27-1*. We generated the *ZmPIP2;5*ΔC deletion mutant and tested its physical interaction with *ZmVAP27-1* by means of BiFC assays. The *ZmPIP2;5*ΔC mutant still interacted with *ZmVAP27-1* (Figs 3b, S2a), suggesting that another *ZmPIP2;5*

cytosolic domain should be involved in the interaction with *ZmVAP27-1*.

#### *ZmPIP2;5* and *ZmVAP27s* are in close vicinity in EPCS and endocytic structures

To study VAP27 protein intracellular localisation relative to the localisation of *ZmPIP2;5*, *ZmVAP27-1* or *ZmVAP27-2* and *ZmPIP2;5* were tagged with mTRQ2 and mVenus, respectively, and transiently expressed in *N. benthamiana* leaves. mTRQ2-*ZmVAP* signals were found close to the PM and around the nucleus in a reticular network, characteristic of the ER (Fig. 4a, b). This was better observed in high magnification images, in which the mTRQ2-*ZmVAP27-1* fluorescent signals were in the cortical ER structure near to the PM and in punctuated structures (Fig. 4c), as previously described for *AVAP27s* present in EPCS (Wang *et al.*, 2014, 2016). The expression of both VAP27s did not modify *ZmPIP2;5* PM localisation (Fig. 4a,b).

PIPs are internalised in response to salt stress (Boursiac *et al.*, 2005; Prak *et al.*, 2008; Pou *et al.*, 2016; Ueda *et al.*, 2016), and VAP27 proteins are involved in endocytic traffic (Stefano *et al.*, 2018). To obtain insights into the nature of the contact between *ZmVAP27-1* with *ZmPIP2;5*, we challenged the cells with a short but strong hyperosmotic salt stress, aiming to plasmolyse the cells but also to observe endocytosis. After 15 min in 4% NaCl,



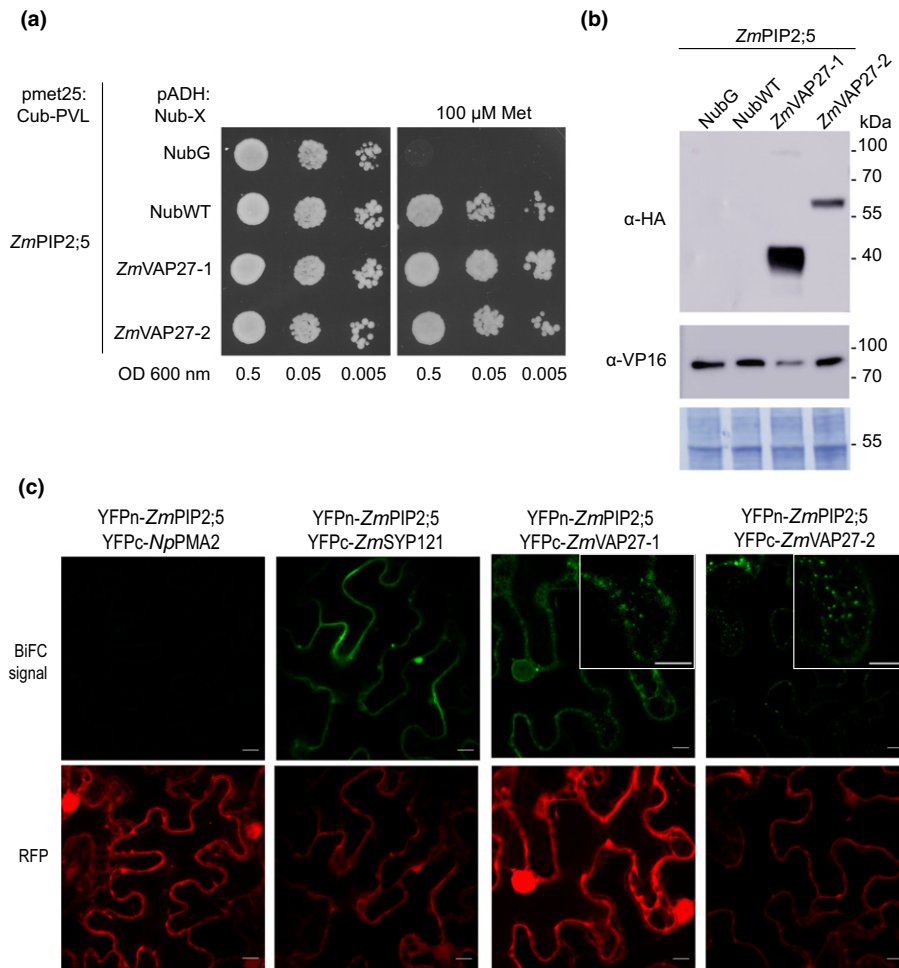


**Fig. 2** *ZmPIP2;5* interacts with *ZmVAP27-1* and *ZmVAP27-2*. (a) Spilt-ubiquitin assay (SUS). Yeast coexpressing the *ZmPIP2;5*-Cub-PLV Met-repressible bait construct and the prey constructs NubG-*ZmVAP27-1*, NubG-*ZmVAP27-2*, NubG, or NubWT were dropped in a dilution series (OD 0.5, 0.05 and 0.005) onto synthetic medium with or without 100 μM methionine to repress bait expression. Yeast growth was recorded after incubation for 48 h. This experiment was repeated with three independent transformed yeast lines for each construct pair. (b) Immunoblot to verify bait and prey fusion protein expression in yeast used for the SUS. The preys were revealed using anti-haemagglutinin (anti-HA) antibody and the bait (*ZmPIP2;5*) was revealed using an anti-VP16 antibody. NubG and NubWT do not contain an HA-tag. The expected molecular weights of the proteins were: NubG-*ZmVAP27-1*, 40 kDa; NubG-*ZmVAP27-2*, 60 kDa, and *ZmPIP2;5*-Cub-PLV, 77 kDa. Polyvinylidene difluoride (PVDF) membrane Coomassie R250 staining (bottom) was used to control the protein loading. (c) Bimolecular fluorescence complementation (BiFC) signals for the pairs YFPn-*ZmPIP2;5*/YFPc-*NpPMA2* (negative control), YFPn-*ZmPIP2;5*/YFPc-*ZmSYP121* (positive control), YFPn-*ZmPIP2;5*/YFPc-*ZmVAP27-1*, YFPn-*ZmPIP2;5*/YFPc-*ZmVAP27-2*. BiFC signal (YFP) is shown in green, and the RFP signal in red serves as a transfection control. Bars, 10 μm. YFP signal was detected with a bright dot pattern for the YFPn-*ZmPIP2;5*/YFPc-*ZmVAP27-1* and YFPn-*ZmPIP2;5*/YFPc-*ZmVAP27-2* pairs (insets).

protoplast detachment from the cell wall occurred and both proteins were detected in Hechtian strands (arrows, Figs 4d,f, S3), which connect the cell wall to the protoplast (Lang-Pauluzzi & Gunning, 2000). Interestingly, characteristic endocytosed intracellular vesicles containing the aquaporin in response to NaCl were surrounded by the mTRQ2-*ZmVAP27-1* signal (arrows, Fig. 4e,g).

To further investigate the interaction between *ZmPIP2;5* and *ZmVAP27-1* we used the Airyscan confocal microscope super-resolution module (Zeiss LSM710). This approach revealed a patched arrangement of mVenus-*ZmPIP2;5* in the PM (Fig. 5a), suggesting that *ZmPIP2;5* organises in PM domains as previously shown for *AtPIP2;1* (Li *et al.*, 2011). This irregular pattern localised partially with the nested arrangement of *ZmVAP27-1* in the ER (Fig. 5a).

Regarding the mVenus-*ZmPIP2;5*-labelled intracellular vesicles that were near to the PM, we were not able to observe mTRQ2 and mVenus signal colocalisation (Fig. 5b). Cell membrane reorganisation upon NaCl treatment highlighted mVenus-*ZmPIP2;5* and mTRQ2-*ZmVAP27-1* colocalisation in Hechtian strands (Fig. 5c,f; zoom out of this panel in Fig. S3b) and *ZmPIP2;5*-labelled vesicles (Fig. 5d,g), as already shown. Also, we detected colocalisation of both proteins in globular structures (Fig. 5e,h), which resemble the PM invaginations labelled with Venus-*AtPIP2;7* induced in response to salt stress conditions (Pou *et al.*, 2016). Additional images showing mVenus-*ZmPIP2;5* and mTRQ2-*ZmVAP27-1* colocalisation upon NaCl stress are shown in Fig. S4. Altogether, these data suggested that *ZmVAP27-1*-labelled ER is organised close to the different structures involved in *ZmPIP2;5* internalisation.

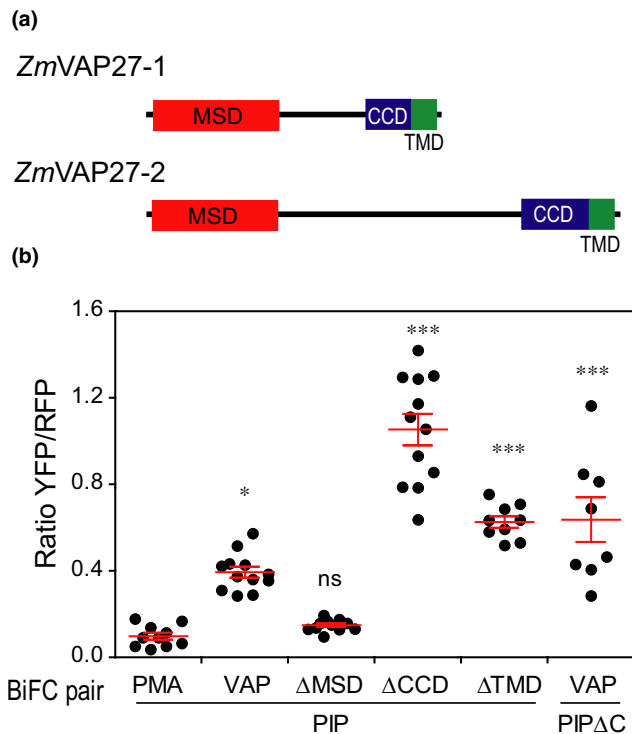


**Fig. 3** *ZmVAP27-1* major sperm domain (MSD) is required for the interaction with *ZmPIP2;5*. (a) Domain composition of the VAP27 proteins that interact with *ZmPIP2;5*. CCD, coiled-coil domain; TMD, transmembrane domain. (b) Fluorescence ratiometric quantification from bimolecular fluorescence complementation (BiFC) experiments with the pairs PIP/PMA (YFPn-*ZmPIP2;5*/YFPc-*NpPMA2*), PIP/VAP (YFPn-*ZmPIP2;5*/YFPc-*ZmVAP27-1*), PIP/ $\Delta$ MSD (YFPn-*ZmPIP2;5*/YFPc-*ZmVAP27-1* $\Delta$ MSD), PIP/ $\Delta$ TMD (YFPn-*ZmPIP2;5*/YFPc-*ZmVAP27-1* $\Delta$ TMD), PIP/ $\Delta$ CCD (YFPn-*ZmPIP2;5*/YFPc-*ZmVAP27-1* $\Delta$ CCD), and PIP $\Delta$ C/VAP (YFPn-*ZmPIP2;5* $\Delta$ C/YFPc-*ZmVAP27-1*). For each scatter plot, the lines indicate the mean  $\pm$  SE. The Kruskal–Wallis and Dunn's multiple comparison test were used to calculate the statistical difference between the negative control and the remaining constructs (\*\*\*,  $P < 0.001$ ; \*,  $P < 0.05$ ; ns, not significant). This experiment was repeated twice.

### *ZmVAP27-1* positively modifies the osmotic membrane water permeability of *ZmPIP2;5* expressing oocytes

To determine whether *ZmVAP27-1* expression modified *ZmPIP2;5* water transport activity, we performed *Xenopus* oocyte swelling assays. Both *ZmPIP2;5* and *ZmVAP27-1* coding cRNAs were injected in oocytes and, after 3 d, the latter was subjected to hypo-osmotic shock. The  $P_f$  values of oocytes injected with *ZmVAP27-1* cRNA alone were not different from the  $P_f$  of NI oocytes, whereas a significant  $P_f$  increase was observed when the oocytes were injected with *ZmPIP2;5* cRNA. *ZmPIP2;5* and *ZmVAP27-1* cRNA co-injection in a 1 : 1 ratio did not modify the mean  $P_f$  value in comparison with *ZmPIP2;5* expression alone. However, the co-injection of *ZmPIP2;5* and *ZmVAP27-1* cRNA in a 1 : 10 ratio caused a mean  $P_f$  value increase over 35% (Figs 6a, S5a,b), indicating a positive synergistic effect on the cell water permeability.

The water permeation through PIP pores is regulated by the cytosolic proton concentration ( $[H^+]_i$ ) (Tournaire-Roux *et al.*,

2003). Under acid conditions, residues located in cytosolic loop D are protonated, and concomitant loop reorganisation leads to PIP pore closure (Törnroth-Horsefield *et al.*, 2006; Frick *et al.*, 2013). A  $P_f$  vs  $[H^+]_i$  sigmoidal curve characterises the cooperative behaviour in proton sensing of the channels that integrate the tetramer (Bellati *et al.*, 2010; Yaneff *et al.*, 2014; Jozefkiewicz *et al.*, 2016). To evaluate if the PIP–VAP27 interaction affected proton sensing, as it may involve PIP cytosolic domains, we compared the relative-  $P_f$  vs  $[H^+]_i$  curves for *ZmPIP2;5* expressed alone and co-expressed with *ZmVAP27-1* (1 : 10) (Fig. 6b; absolute  $P_f$  values reported in Fig. S5c,d). The  $[H^+]_{0.5}$  remained constant among the assays ( $0.21 \pm 0.02$  vs  $0.24 \pm 0.01$ , mean  $\pm$  standard error (SE),  $n = 2$ ), suggesting that the interaction between *ZmPIP2;5* and *ZmVAP27-1* did not alter the aquaporin structural elements involved in pH sensing.

### The PIP2–VAP27 interaction is conserved among different angiosperms

Currently our understanding about plant VAPs mainly arises from research in the plant model *Arabidopsis* (Wang *et al.*, 2014, 2016; Pérez-Sancho *et al.*, 2015), whereas maize VAP proteins have not been characterised yet. Intending to better understand the PIP–VAP27 interaction we identified maize VAPs and studied VAP27 phylogeny in green plants (Viridiplantae). We identified 19 proteins containing a MSD in the B73 maize genome (Fig. S6a). The MSD is a conserved feature among VAPs, but proteins from other families may also contain this domain. Indeed, 17 of the 19 proteins were homologues of the previously characterised *AtVAP27s*, whereas the remaining two proteins were unrelated to VAP27s. The *ZmPIP2;5* interactors (*ZmVAP27-1* and *ZmVAP27-2*) are part of the same homology group with an MSD amino acid sequence identity over 50% (Fig. S6b). Publicly available transcriptome data analysis showed that six of 14 group members are highly expressed in most plant tissues (Fig. S6c). Both *ZmVAP27-1* and *ZmVAP27-2* are among these highly expressed genes, and exhibit the greatest expression levels in roots (Fig. S6c), similar to *ZmPIP2;5* (Hachez *et al.*, 2006, 2008).

To obtain insights into the family evolution of the *ZmVAP27-1* and *ZmVAP27-2* homology group, we performed a phylogenetic analysis. A balanced selection of species and genes allowed an alignment of 254 proteins from 41 green plant species (see Materials and methods section). The reconstructed phylogenetic tree showed that this VAP27 homology group can be further subdivided into two paralogue groups (Fig. 7a, the full phylogeny is shown in Fig. S7), which correspond with the previously defined *AtVAP27s* clades I and III (Wang *et al.*, 2016). The presence of these clades can be traced back to Gymnosperms, suggesting that both clades were present in the Spermatophyta ancestor. Within each of these two main clades, two subgroups can be distinguished for Angiosperms, showing family-specific expansion events. *ZmVAP27-1*, together with other seven *ZmVAP27s*, clearly group in the *AtVAP27* clade I, the closer *Arabidopsis* *ZmVAP27-1* orthologues being the isoforms *AtVAP27-1/3/5/7*.



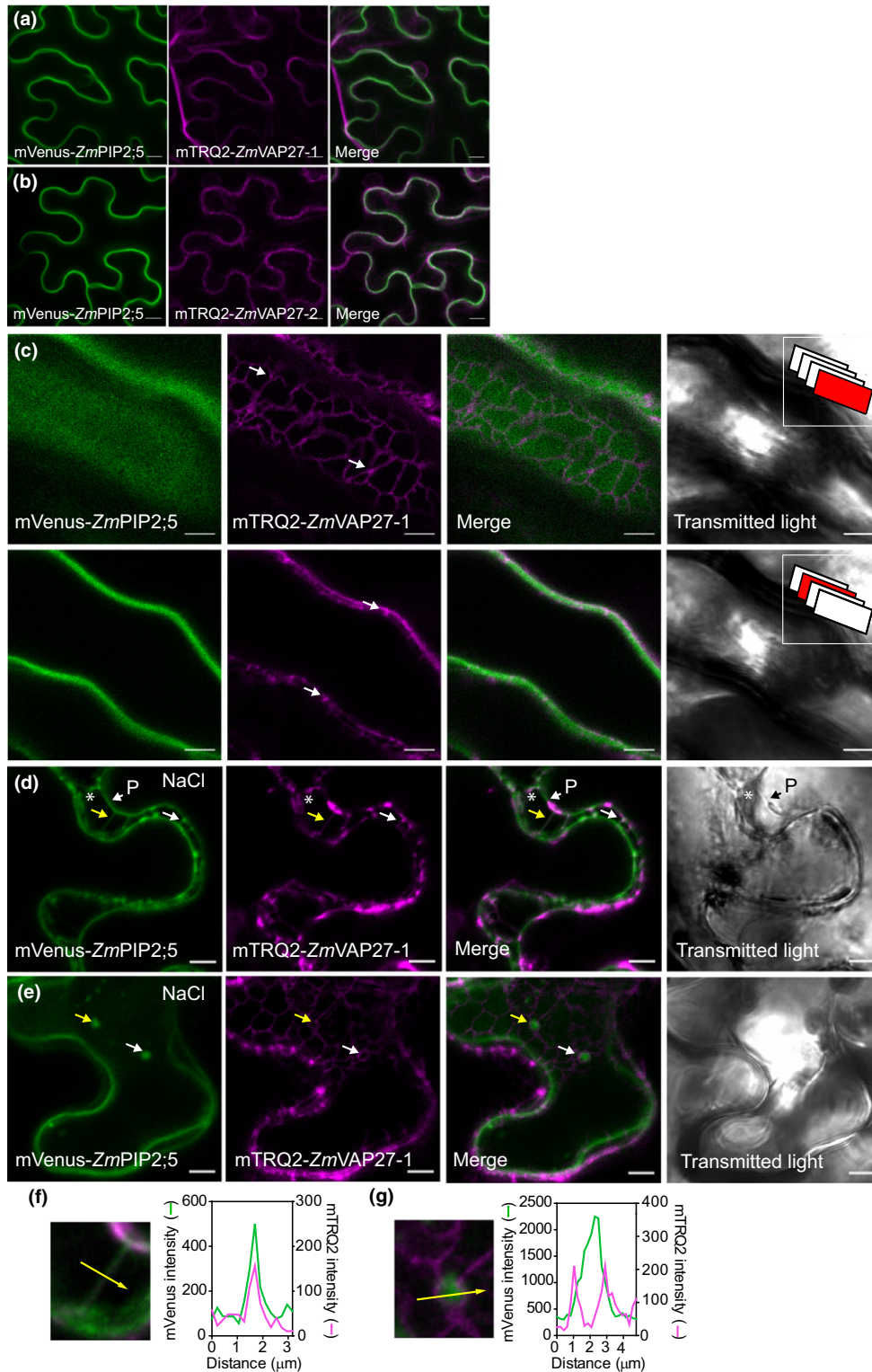


**Fig. 4** *ZmVAP27-1* and *ZmVAP27-2* are in the endoplasmic reticulum (ER) in close proximity to the plasma membrane (PM)-localised *ZmPIP2;5*. (a, b) Confocal images (Z-stack projection) of tobacco leaf cells transiently overexpressing mVenus-*ZmPIP2;5* and mTRQ2-*ZmVAP27-1* (a) or mVenus-*ZmPIP2;5* and mTRQ2-*ZmVAP27-2* (b). Bars, 10 μm. (c) Inset in two confocal planes of cells overexpressing mVenus-*ZmPIP2;5* and mTRQ2-*ZmVAP27-1*. Insets in the transmitted light panels represent in red the scanned plane (1.02 μm thin) position in the Z-stack. Arrows point to VAP27 dots. (d, e) Confocal images of cells overexpressing mVenus-*ZmPIP2;5* and mTRQ2-*ZmVAP27-1* after treatment with NaCl (4%) for 15 min. (d) Arrows point to Hetchian strands, asterisks indicate the periplasmic space, and P is the receding protoplast. Arrows in (e) point to mVenus-*ZmPIP2;5* vesicles surrounded by mTRQ2 signal. (f, g) Insets and fluorescence intensity profiles (arbitrary units) for mVenus and mTRQ2 in the structures pointed out with the yellow arrows in (d, e): an Hetchian strand (f), and endocytic vesicle (g). Bars, 5 μm.

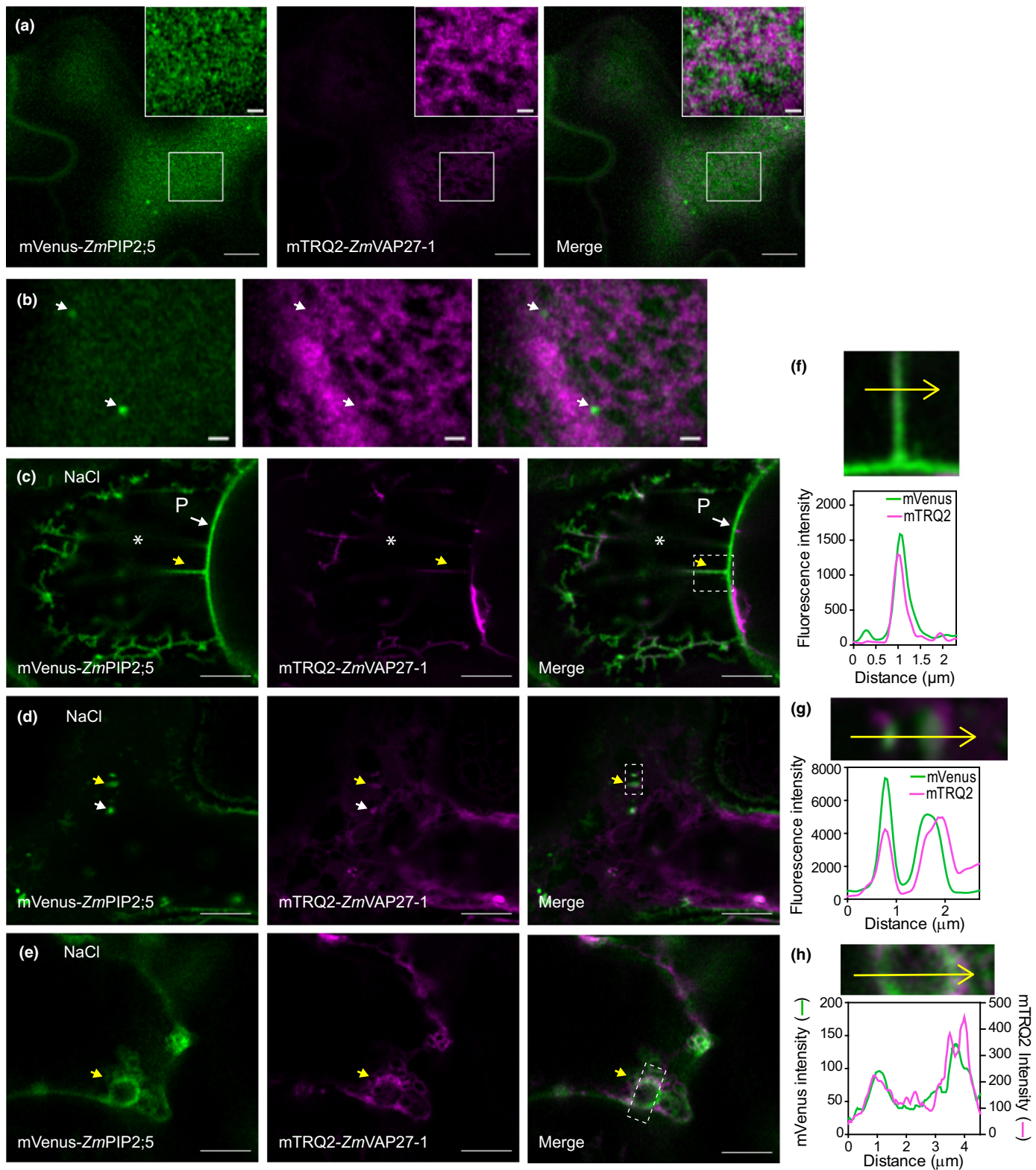


**Fig. 5** *ZmVAP27-1* colocalises with *ZmPIP2;5* in NaCl stress-related structures. (a) Airyscan confocal images of cells overexpressing mVenus-*ZmPIP2;5* and mTRQ2-*ZmVAP27-1*. Bars, 5  $\mu\text{m}$ . Inset bars, 1  $\mu\text{m}$ . (b) Airyscan confocal images of the same cell as in (a), but a different Z-position. Bars, 1  $\mu\text{m}$ . (c–e) Airyscan confocal images of cells overexpressing mVenus-*ZmPIP2;5* and mTRQ2-*ZmVAP27-1* after treatment with NaCl (4%) for 15 min. (c) P, the receding protoplast, asterisks indicate to the periplasmic space. Arrows point to NaCl-induced: Hetchian strands (c), endocytic vesicles (d), and globular structure (e). (f–h) Insets and fluorescence intensity profiles (arbitrary units) for mVenus and mTRQ2 in the structures pointed with the yellow arrows in (c–e): an Hetchian strand (f), endocytic vesicles (g), and globular structure (h). Bars, 5  $\mu\text{m}$ .



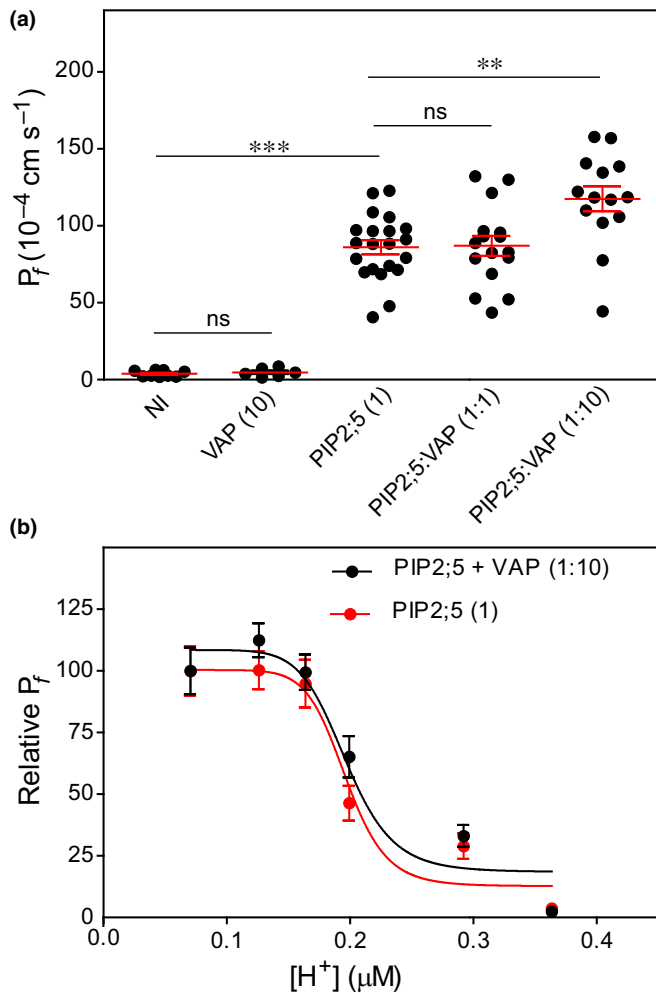


**Fig. 6** *ZmVAP27-1* increases *Xenopus* oocyte  $P_f$  when co-expressed with *ZmPIP2;5*. (a) Water permeability coefficient ( $P_f$ ) of noninjected oocytes (NI, control) or injected with *ZmVAP27-1* cRNA alone (7.5 ng), *ZmPIP2;5* cRNA alone (0.75 ng), or coinjected with both cRNAs in different mass ratios (1 : 1 or 1 : 10). For each scatter plot the lines indicate the mean  $\pm$  SE. ANOVA and Bonferroni's multiple comparison test were used to calculate the statistical difference between treatments (\*\*\*,  $P < 0.001$ ; \*\*,  $P < 0.01$ ; ns, not significant). The differences reported here were observed with three independent oocyte batches. (b) Relative  $P_f$  after cytosolic acidification tested in oocytes injected with *ZmPIP2;5* cRNA alone (0.75 ng), or with *ZmPIP2;5* (0.75 ng) and *ZmVAP27-1* (7.5 ng) cRNAs (1 : 10 ratio). Data points are representative values obtained from the same oocyte batch (mean relative  $P_f \pm$  SE). This is one representative experiment of two independent experiments.

Conversely, *ZmVAP27-2*, and five other *ZmVAP27*s, group with the *AtVAP27* clade III, the closer Arabidopsis *ZmVAP27-2* orthologue being the isoform *AtVAP27-2* (Fig. 7a).

Regarding PIP2 channel evolution, their origin can be traced back to the Embryophyta ancestor (Soto *et al.*, 2012; Abascal *et al.*, 2014). We hypothesised that the PIP2–VAP27 interaction is conserved through evolution. We looked for evidence to support this hypothesis in the published Arabidopsis data. We localised in the Arabidopsis Interactome Map (Consortium, 2011) *AtVAP27-1* interaction with *AtPIP2;3*, *AtPIP2;7*, and *AtPIP2;8* and the interaction of *AtVAP27-4* with *AtPIP2;7*. Also, the *AtVAP27-3* isoform was pulled-down with *AtPIP2;1* and not

with *AtPIP1;2* (Bellati *et al.*, 2016). We validated the interaction between *AtPIP2;7* and *AtVAP27-1* by BiFC (Fig. 7b), and we also tested whether *AtPIP2;7* was able to interact with *ZmVAP27-1*. As observed in Fig. 7(b), co-expression of both proteins led to a fluorescent signal, demonstrating their interaction. Altogether, these data showed that the PIP2–VAP27 interaction is an ancient land plant feature, being at least present in the common Angiosperm ancestor. Future work will elucidate whether this interaction is also present in bryophytes, or if it is a distinctive vascular plant feature.

## Discussion

To unravel the different aquaporin roles and regulation mechanisms in water and/or solute homeostasis in plant cells, it is crucial to identify their intracellular partners. The pull-down assays presented here, together with previous assays using tagged PIPs (Hachez *et al.*, 2014a; Bellati *et al.*, 2016), allowed protein identification from the cytoskeleton and ER as PIP partners (Table S4), suggesting a close interaction between PIPs and those cellular structures. Moreover, we showed that PIP2s and the ER resident VAP27s interact, and presented novel evidence of plant aquaporin activity regulation by EPC residents.

To our knowledge, *ZmPIP2;5* is the first plant PM protein identified as a partner of ER-located VAP27s. We confirmed these interactions by SUS and BiFC experiments (Fig. 2). Interestingly, ER-located VAP27s are anchored to the cell wall by unknown PM proteins (Wang *et al.*, 2016). We speculate that *ZmPIP2;5* might be one of the proteins anchoring ER-located *ZmVAP27*s to the cell wall. Actually, the cell wall restricts *AtPIP2;1* mobility (Martiniere *et al.*, 2012) and, using fluorescence recovery after photobleaching assays (Methods S2), we also showed that *ZmPIP2;5* mobility in the PM is restricted in comparison with other proteins that expose few amino acids to the apoplast, like *ZmLTI6A* (Fig. S8). Also, we demonstrated that the *ZmVAP27-1* MSD is essential for the PIP–VAP27 interaction, whereas the CCD and TMD are not (Fig. 3b). It is important to point out that *ZmPIP2;5* and *ZmSYP121* are both PM residents and their BiFC signals reconstitute at the PM, whereas the BiFC signal of the *ZmPIP2;5*–*ZmVAP27-1/2* pairs reconstitutes in dotted structures (Fig. 2c), reminiscent of the *AtVAP27-1* bright dotted pattern (Wang *et al.*, 2016). Conversely, mTRQ2–*ZmVAP27-1/2* expression in the ER did not prevent mVenus–*ZmPIP2;5* PM localisation (Figs 4, 5). These results, together with the central role of the MSD in the interaction, demonstrate that the interaction between VAP27-1/2 and *ZmPIP2;5* occurs at EPCs. We also showed that *AtVAP27-1* interacted with *AtPIP2;7* (Fig. 7), and *AtVAP27-3* was also detected in an *AtPIP2;1* interactomic study performed by Bellati *et al.* (2016). All these observations, together with the fact that *ZmVAP27-1* was not interacting in BiFC assays with the  $H^+$ -ATPase PMA2 (Fig. S1), another protein that is enriched in PM microdomains just like PIP channels (Laloi *et al.*, 2007), might indicate that PIP aquaporins play a role in anchoring the EPCs to the cell wall.

Endocytosis is a rapid way to adjust PIP protein abundance in the PM in response to an osmotic or salt stress (Chaumont &



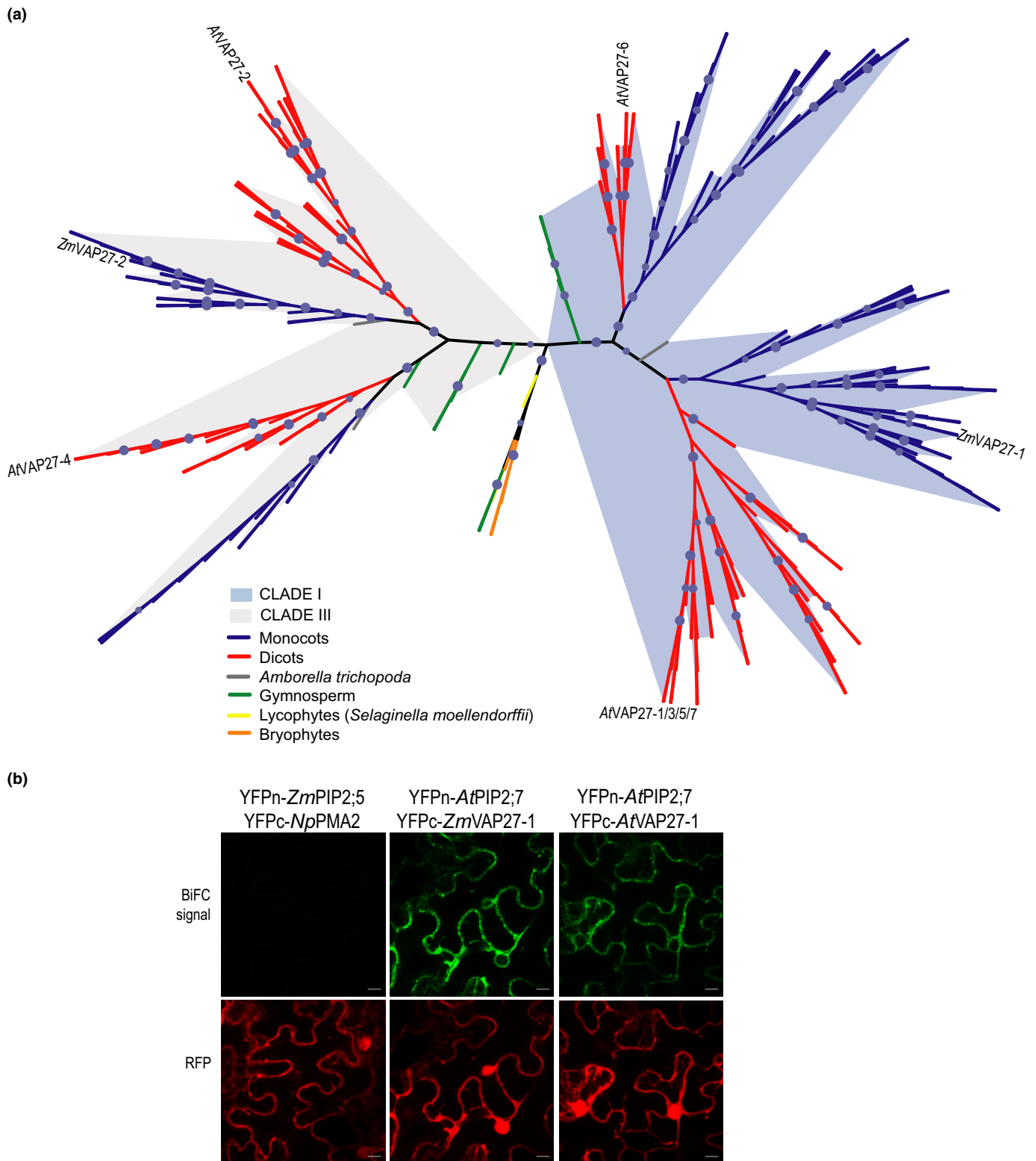


**Fig. 7** VAP27 protein phylogenetic analysis and conservation of the PIP–VAP27 interaction in Arabidopsis. (a) *ZmVAP27-1* and *ZmVAP27-2* homology group phylogenetic tree reconstructed by maximum likelihood. Branch support was assessed by the ultrafast bootstrap approximation with 1000 replicates (values  $\geq 95$  are represented by a blue circle). Maize VAP27-1, VAP27-2 and Arabidopsis VAP27s are shown in the tree. Branches are coloured according to the taxonomy in the accompanying legends. The shadows emphasise the expansion of two different clades. (b) AtPIP2;7 interacts with the Arabidopsis and maize VAP27-1 proteins. Bimolecular fluorescence complementation (BiFC) signals for the pairs YFPn-ZmPIP2;5/YFPc-NpPMA2 (negative control), YFPn-AtPIP2;7/YFPc-ZmVAP27-1, and YFPn-AtPIP2;7/YFPc-AtVAP27-1. BiFC signal (YFP) is in green, and the RFP signal is in red and serves as a transfection control. Bars, 10  $\mu$ m.

Tyerman, 2014; Pou *et al.*, 2016). Salt stress-induced *AtPIP2*;1 internalisation is a process that depends on two kinases: phosphatidylinositol 3-kinase (PI3K) and phosphatidylinositol 4-kinase (PI4K) (Ueda *et al.*, 2016). Interestingly, *AtVAP27-1/3* bind with high affinity to different phosphorylated PI (Stefano *et al.*, 2018), among them the PI3K and PI4K products. In addition, endocytosis is partially impaired in the plant double mutant *vap27-1/vap27-3* (Stefano *et al.*, 2018), as it is impaired in mammal cells lacking VAPs (Dong *et al.*, 2016). Here, we showed that salt stress-induced vesicles carrying *ZmPIP2*;5 are wrapped with *ZmVAP27-1*-labelled ER (Figs 4e, 5d,e). Therefore, PIP interaction with VAP27s can facilitate PIP loading into endocytic structures enriched in specific PIs.

Upon osmotic stress, *AtPIP2*;7 interaction with the tryptophan-rich sensory protein/translocator (TSPO) leads to aquaporin level reduction in the PM, through degradation by the autophagic pathway (Hachez *et al.*, 2014b; Jurkiewicz *et al.*, 2020). How the internalisation of this complex occurs is still unknown. Interestingly, TSPO and PIP interaction occurs only if TSPO binds PI(4,5)P2 (Jurkiewicz *et al.*, 2020) and VAP27s also bind PI(4,5)P2 (Stefano *et al.*, 2018). Moreover, *AtVAP27-1* interacts with essential proteins involved in endocytic component autophagy (Wang & Hussey, 2019). As *AtPIP2*;7 interacts with *AtVAP27-1* (Fig. 7b), we propose that PIP autophagy may be initiated at EPCs through its interaction with TSPO and VAP27s. This hypothesis will need to be addressed.

The PIP–VAP27 interaction increases oocyte membrane water permeability compared with oocytes expressing PIP alone (Fig. 6a). We found no evidence of a modification in PIP proton sensing by VAP27s (Fig. 6b), suggesting that the structural elements involved in pH sensing are not affected by the interaction. Still, we cannot discard a conformational pore modification. Therefore, the  $P_f$  increase could be explained either by a greater intrinsic permeability of PIP channels due to a conducting pore conformational change, or by a greater active channel number in the PM. Under normal conditions, when no stress signals are perceived by cells to induce PIP internalisation, VAP27s could recruit and stabilise the channels in EPCs similar to the VAPs clustering of the mammal potassium channel Kv2.1 (Kirmiz *et al.*, 2018). Interestingly, cells with genetically elevated PI(4,5)P2 levels also have greater  $P_f$  than control cells (Ma *et al.*, 2015). The authors were able to link the PI effect on  $P_f$  to aquaporins, but they were not able to discern between an increase in channel abundance in the PM or an increase in their water channel activity. Further research will help to understand if VAP27s stabilise PIPs in the PM and guide the channels to rapid endocytosis in response to a stimulus.

We recently reported how *ZmPIP2*;5 expression levels affect water relationships and plant growth (Ding *et al.*, 2020). *ZmPIP2*;5 is the most highly expressed PIP2 isoform in roots. Interestingly, the two different *ZmVAP27s* that interact with *ZmPIP2*;5 are also highly expressed in roots (Fig. S6c), and belong to different clades that we traced back to the Spermatophyta ancestor (*c.* 319 million years ago (Ma); Jiao *et al.*, 2011) (Fig. 7a). The challenge of future research will be to understand: (1) the role of the interaction in plant water movement, especially

in response to osmotic and salt stress; (2) whether these interactions are linked to the acquisition of new functionalities *in planta*; and (3) whether the *ZmPIP2*;5/*ZmVAP27-1* and *ZmPIP2*;5/*ZmVAP27-2* interactions form part of different EPCs types or not.






## Acknowledgements

We thank MASSPROT, IMABIOL, Marie-Christine Eloy for confocal expertise and Joseph Nader for his helpful advice in benchwork. This work was supported by the Belgian National Fund for Scientific Research (FNRS, FRFC 2.4.501.06F), the ‘Communauté française de Belgique-Actions de Recherches Concertées’ (grant ARC16/21-075), the Pierre and Colette Bauchau Award, the Consejo Nacional de Investigaciones Científicas y Técnicas (CONICET PIP 2014-0206), and the Agencia Nacional de Promoción Científica y Tecnológica (PICT 2017-0244). ARF was supported by an Incoming Post-doc Move-in Louvain Fellowship co-funded by the Marie Curie Actions. FS was supported by a research fellow at the Universidad de Buenos Aires. TL was supported by a research fellow at the Fonds de Formation à la Recherche dans l’Industrie et l’Agriculture.

## Author contributions

ARF and FC designed the experiments. ARF, TL, FS, KF and HD performed the experiments. ARF, TL, FS, HD, PM, KA and FC analysed the data. ARF and FC wrote the manuscript. All the authors contributed to the discussion and revision of the manuscript.

## ORCID

Karina Alleva  <https://orcid.org/0000-0002-9081-2103>  
 François Chaumont  <https://orcid.org/0000-0003-0155-7778>  
 Karolina Filik  <https://orcid.org/0000-0002-8086-038X>  
 Pierre Morsomme  <https://orcid.org/0000-0001-7780-7230>  
 Ana Romina Fox  <https://orcid.org/0000-0002-7852-4539>

## References

- Abascal F, Irisarri I, Zardoya R. 2014. Diversity and evolution of membrane intrinsic proteins. *Biochimica et Biophysica Acta* 1840: 1468–1481.
- Afzal Z, Howton T, Sun Y, Mukhtar M. 2016. The roles of aquaporins in plant stress responses. *Journal of Developmental Biology* 4: 9.
- Batoko H, Zheng H-Q, Hawes C, Moore I. 2000. A Rab1 GTPase is required for transport between the endoplasmic reticulum and golgi apparatus and for normal golgi movement in plants. *Plant Cell* 12: 2201.
- Bellati J, Alleva K, Soto G, Vitali V, Jozefkovic C, Amodeo G. 2010. Intracellular pH sensing is altered by plasma membrane PIP aquaporin co-expression. *Plant Molecular Biology* 74: 105–118.
- Bellati J, Champeyroux C, Hem S, Rofidal V, Krouk G, Maurel C, Santoni V. 2016. Novel aquaporin regulatory mechanisms revealed by interactomics. *Molecular & Cellular Proteomics* 15: 3473–3487.
- Besserer A, Burnotte E, Bienert GP, Chevalier AS, Errachid A, Grefen C, Blatt MR, Chaumont F. 2012. Selective regulation of maize plasma membrane aquaporin trafficking and activity by the SNARE SYP121. *Plant Cell* 24: 3463.

- Bienert GP, Heinen RB, Berny MC, Chaumont F. 2014. Maize plasma membrane aquaporin *ZmPIP2;5*, but not *ZmPIP1;2*, facilitates transmembrane diffusion of hydrogen peroxide. *Biochimica et Biophysica Acta – Biomembranes* 1838: 216–222.
- Boursiac Y, Chen S, Luu D-T, Sorrieu M, van den Dries N, Maurel C. 2005. Early effects of salinity on water transport in Arabidopsis roots. Molecular and cellular features of aquaporin expression. *Plant Physiology* 139: 790–805.
- Bradford MM. 1976. A rapid and sensitive method for the quantitation of microgram quantities of protein utilizing the principle of protein-dye binding. *Analytical Biochemistry* 72: 248–254.
- Capella-Gutierrez S, Silla-Martinez JM, Gabaldon T. 2009. trimAl: a tool for automated alignment trimming in large-scale phylogenetic analyses. *Bioinformatics* 25: 1972–1973.
- Chaumont F, Tyerman SD. 2014. Aquaporins: highly regulated channels controlling plant water relations. *Plant Physiology* 164: 1600–1618.
- Chevalier AS, Bienert GP, Chaumont F. 2014. A new LxxxA motif in the transmembrane Helix3 of maize aquaporins belonging to the plasma membrane intrinsic protein PIP2 group is required for their trafficking to the plasma membrane. *Plant Physiology* 166: 125–138.
- Consortium AIM. 2011. Evidence for network evolution in an Arabidopsis interactome map. *Science* 333: 601–607.
- Deeks MJ, Calcutt JR, Ingle EKS, Hawkins TJ, Chapman S, Richardson AC, Mentlak DA, Dixon MR, Cartwright F, Smertenko AP *et al.* 2012. A superfamily of actin-binding proteins at the actin-membrane nexus of higher plants. *Current Biology* 22: 1595–1600.
- Ding L, Milhiet T, Couvreur V, Nelissen H, Meziane A, Parent B, Aesaert S, Lijsebettens MV, Inzé D, Tardieu F *et al.* 2020. Modification of the expression of the aquaporin *ZmPIP2;5* affects water relations and plant growth. *Plant Physiology* 182: 2154–2165.
- Dong R, Saheki Y, Swarup S, Lucast L, Harper JW, De Camilli P. 2016. Endosome-ER contacts control actin nucleation and retromer function through VAP-dependent regulation of PI4P. *Cell* 166: 408–423.
- Fortuna AC, Palma GZD, Car LA, Armentia L, Vitali V, Zeida A, Estrin DA, Alleva K. 2019. Gating in plant plasma membrane aquaporins: the involvement of leucine in the formation of a pore constriction in the closed state. *FEBS Journal* 286: 3473–3487.
- Fox AR, Maistriaux LC, Chaumont F. 2017. Toward understanding of the high number of plant aquaporin isoforms and multiple regulation mechanisms. *Plant Science* 264: 179–187.
- Frick A, Järva M, Törnroth-Horsefield S. 2013. Structural basis for pH gating of plant aquaporins. *FEBS Letters* 587: 989–993.
- Glaab E, Schneider R. 2015. RepExplore: addressing technical replicate variance in proteomics and metabolomics data analysis. *Bioinformatics* 31: 2235–2237.
- Goldman A, Harper S, Speicher DW. 2016. Detection of proteins on blot membranes. *Current Protocols in Protein Science* 86: 1–10.
- Gorgoni B, Fiorentino L, Marchioni M, Carnevali F. 1995. Cloning, expression and functional role of XRPF1  $\alpha$  and  $\beta$  subunits in *Xenopus laevis* oocyte. *Biochemical and Biophysical Research Communications* 215: 1088–1095.
- Grefen C, Blatt MR. 2012. A 2in1 cloning system enables ratiometric bimolecular fluorescence complementation (rBiFC). *BioTechniques* 53: 311–314.
- Grefen C, Obrdlík P, Harter K. 2009. The determination of protein-protein interactions by the mating-based split-ubiquitin system (mbsUS). *Methods in Molecular Biology (Clifton, N.J.)* 479: 217–233.
- Gronin A, Rodrigues O, Verdoucq L, Merlot S, Leonhardt N, Maurel C. 2015. Aquaporins contribute to ABA-triggered stomatal closure through OST1-mediated phosphorylation. *Plant Cell* 27: 1945–1954.
- Guindon S, Dufayard J-F, Lefort V, Anisimova M, Hordijk W, Gascuel O. 2010. New algorithms and methods to estimate maximum-likelihood phylogenies: assessing the performance of PhyML 3.0. *Systematic Biology* 59: 307–321.
- Hachez C, Heinen RB, Draye X, Chaumont F. 2008. The expression pattern of plasma membrane aquaporins in maize leaf highlights their role in hydraulic regulation. *Plant Molecular Biology* 68: 337.
- Hachez C, Laloux T, Reinhardt H, Cavez D, Degand H, Grefen C, Rycke RD, Inzé D, Blatt MR, Russinova E *et al.* 2014a. Arabidopsis SNAREs SYP61 and SYP121 coordinate the trafficking of plasma membrane aquaporin PIP2;7 to modulate the cell membrane water permeability. *Plant Cell* 26: 3132–3147.
- Hachez C, Moshelion M, Zelazny E, Cavez D, Chaumont F. 2006. Localization and quantification of plasma membrane aquaporin expression in maize primary root: A clue to understanding their role as cellular plumbers. *Plant Molecular Biology* 62: 305–323.
- Hachez C, Veljanovski V, Reinhardt H, Guillaumont D, Vanhee C, Chaumont F, Batoko H. 2014b. The Arabidopsis abiotic stress-induced TSPO-related protein reduces cell-surface expression of the aquaporin PIP2;7 through protein-protein interactions and autophagic degradation. *Plant Cell* 26: 4974–4990.
- Hecker A, Wallmeroth N, Peter S, Blatt MR, Harter K, Grefen C. 2015. Binary 2in1 vectors improve *in planta* (co)localization and dynamic protein interaction studies. *Plant Physiology* 168: 776–787.
- Heinen RB, Ye Q, Chaumont F. 2009. Role of aquaporins in leaf physiology. *Journal of Experimental Botany* 60: 2971–2985.
- Hoang DT, Chernomor O, von Haeseler A, Minh BQ, Vinh LS. 2018. UFBoot2: improving the ultrafast bootstrap approximation. *Molecular Biology and Evolution* 35: 518–522.
- Hosy E, Martinière A, Choquet D, Maurel C, Luu D-T. 2015. Super-resolved and dynamic imaging of membrane proteins in plant cells reveal contrasting kinetic profiles and multiple confinement mechanisms. *Molecular Plant* 8: 339–342.
- Jiao Y, Wickett NJ, Ayyampalayam S, Chanderbali AS, Landherr L, Ralph PE, Tomsho LP, Hu Y, Liang H, Soltis PS *et al.* 2011. Ancestral polyploidy in seed plants and angiosperms. *Nature* 473: 97–100.
- Johnson B, Leek AN, Solé L, Maverick EE, Levine TP, Tamkun MM. 2018. Kv2 potassium channels form endoplasmic reticulum/plasma membrane junctions via interaction with VAPA and VAPB. *Proceedings of the National Academy of Sciences, USA* 115: E7331–E7340.
- Jozefkiewicz C, Rosi P, Sigaut L, Soto G, Pietrasanta LI, Amodeo G, Alleva K. 2013. Loop A is critical for the functional interaction of two *Beta vulgaris* PIP aquaporins. *PLoS ONE* 8: e57993.
- Jozefkiewicz C, Sigaut L, Scochera F, Soto G, Ayub N, Pietrasanta LI, Amodeo G, González Flecha FL, Alleva K. 2016. PIP water transport and its pH dependence are regulated by tetramer stoichiometry. *Biophysical Journal* 110: 1312–1321.
- Jurkiewicz P, Senicourt L, Ayeb H, Lequin O, Lacapere J-J, Batoko H. 2020. A plant-specific N-terminal extension reveals evolutionary functional divergence within translocator proteins. *iScience* 23: 100889.
- Kalyaanamoorthy S, Minh BQ, Wong TKF, von Haeseler A, Jermiin LS. 2017. ModelFinder: fast model selection for accurate phylogenetic estimates. *Nature Methods* 14: 587–589.
- Kim H, Kwon H, Kim S, Kim MK, Botella MA, Yun HS, Kwon C. 2016. Synaptotagmin 1 negatively controls the two distinct immune secretory pathways to powdery mildew fungi in Arabidopsis. *Plant and Cell Physiology* 57: 1133–1141.
- Kirik V, Herrmann U, Parupalli C, Sedbrook JC, Ehrhardt DW, Hülskamp M. 2007. CLASP localizes in two discrete patterns on cortical microtubules and is required for cell morphogenesis and cell division in Arabidopsis. *Journal of Cell Science* 120: 4416–4425.
- Kirmiz M, Vierra NC, Palacio S, Trimmer JS. 2018. Identification of VAPA and VAPB as Kv2 channel-interacting proteins defining endoplasmic reticulum-plasma membrane junctions in mammalian brain neurons. *Journal of Neuroscience* 38: 7562–7584.
- Krtková J, Benáková M, Schwarzerová K. 2016. Multifunctional microtubule-associated proteins in plants. *Frontiers in Plant Science* 7: 474.
- Laloi M, Perret A-M, Chatre L, Melsner S, Cantrel C, Vaultier M-N, Zachowski A, Bathany K, Schmitter J-M, Vallet M *et al.* 2007. Insights into the role of specific lipids in the formation and delivery of lipid microdomains to the plasma membrane of plant cells. *Plant Physiology* 143: 461–472.
- Lang-Pauluzzi I, Gunning BES. 2000. A plasmolytic cycle: The fate of cytoskeletal elements. *Protoplasma* 212: 174–185.
- Lee E, Vanneste S, Pérez-Sancho J, Benitez-Fuente F, Strelau M, Macho AP, Botella MA, Friml J, Rosado A. 2019. Ionic stress enhances ER-PM connectivity via phosphoinositide-associated SYT1 contact site expansion in Arabidopsis. *Proceedings of the National Academy of Sciences, USA* 116: 1420–1429.
- Lee HK, Cho SK, Son O, Xu Z, Hwang I, Kim WT. 2009. Drought stress-induced Rma1H1, a RING membrane-anchor E3 ubiquitin ligase homolog,



- regulates aquaporin levels via ubiquitination in transgenic Arabidopsis plants. *Plant Cell* 21: 622–641.
- Letunic I, Bork P. 2016. Interactive tree of life (iTOL) v3: an online tool for the display and annotation of phylogenetic and other trees. *Nucleic Acids Research* 44: W242–W245.
- Lewis JD, Lazarowitz SG. 2010. Arabidopsis synaptotagmin SYTA regulates endocytosis and virus movement protein cell-to-cell transport. *Proceedings of the National Academy of Sciences, USA* 107: 2491–2496.
- Li L, Wang H, Gago J, Cui H, Qian Z, Kodama N, Ji H, Tian S, Shen D, Chen Y *et al.* 2015. Harpin Hpa1 interacts with aquaporin PIP1;4 to promote the substrate transport and photosynthesis in Arabidopsis. *Scientific Reports* 5: 17207.
- Li X, Wang X, Yang Y, Li R, He Q, Fang X, Luu D-T, Maurel C, Lin J. 2011. Single-molecule analysis of PIP2;1 dynamics and partitioning reveals multiple modes of Arabidopsis plasma membrane aquaporin regulation. *Plant Cell* 23: 3780–3797.
- Martiniere A, Lavagi I, Nageswaran G, Rolfe DJ, Maneta-Peyret L, Luu D-T, Botchway SW, Webb SED, Mongrand S, Maurel C *et al.* 2012. Cell wall constrains lateral diffusion of plant plasma-membrane proteins. *Proceedings of the National Academy of Sciences, USA* 109: 12805–12810.
- Maurel C, Boursiac Y, Luu D-T, Santoni V, Shahzad Z, Verdoucq L. 2015. Aquaporins in plants. *Physiological Reviews* 95: 1321–1358.
- Ma X, Shatil-Cohen A, Ben-Dor S, Wigoda N, Perera IY, Im YJ, Diminshtein S, Yu L, Boss WF, Moshelion M *et al.* 2015. Do phosphoinositides regulate membrane water permeability of tobacco protoplasts by enhancing the aquaporin pathway? *Planta* 241: 741–755.
- McFarlane HE, Lee EK, van Bezouwen LS, Ross B, Rosado A, Samuels AL. 2017. Multiscale structural analysis of plant ER–PM contact sites. *Plant and Cell Physiology* 58: 478–484.
- Moshelion M, Moran N, Chaumont F. 2004. Dynamic changes in the osmotic water permeability of protoplast plasma membrane. *Plant Physiology* 135: 2301–2317.
- Murphy SE, Levine TP. 2016. VAP, a versatile access point for the endoplasmic reticulum: review and analysis of FFAT-like motifs in the VAPome. *Biochimica et Biophysica Acta – Molecular and Cell Biology of Lipids* 1861: 952–961.
- Paredes AR, Somerville CR, Ehrhardt DW. 2006. Visualization of cellulose synthase demonstrates functional association with microtubules. *Science* 312: 1491–1495.
- Pérez-Sancho J, Tilsner J, Samuels AL, Botella MA, Bayer EM, Rosado A. 2016. Stitching organelles: organization and function of specialized membrane contact sites in plants. *Trends in Cell Biology* 26: 705–717.
- Pérez-Sancho J, Vanneste S, Lee E, McFarlane HE, del Valle AE, Valpuesta V, Friml J, Botella MA, Rosado A. 2015. The Arabidopsis synaptotagmin I is enriched in endoplasmic reticulum-plasma membrane contact sites and confers cellular resistance to mechanical stresses. *Plant Physiology* 168: 132–143.
- Pietra S, Gustavsson A, Kiefer C, Kalmbach L, Hörstedt P, Ikeda Y, Stepanova AN, Alonso JM, Grebe M. 2013. Arabidopsis SABRE and CLASP interact to stabilize cell division plane orientation and planar polarity. *Nature Communications* 4: 2779.
- Pou A, Jeanguenin L, Milhiet T, Batoko H, Chaumont F, Hachez C. 2016. Salinity-mediated transcriptional and post-translational regulation of the Arabidopsis aquaporin PIP2;7. *Plant Molecular Biology* 92: 731–744.
- Prak S, Hem S, Boudet J, Viennois G, Sommerer N, Rossignol M, Maurel C, Santoni V. 2008. Multiple phosphorylations in the C-terminal tail of plant plasma membrane aquaporins: Role in subcellular trafficking of *At* PIP2;1 in response to salt stress. *Molecular & Cellular Proteomics* 7: 1019–1030.
- Roche JV, Törnroth-Horsefield S. 2017. Aquaporin protein–protein interactions. *International Journal of Molecular Sciences* 18: 2255.
- Schultz J, Milpetz F, Bork P, Ponting CP. 1998. SMART, a simple modular architecture research tool: identification of signaling domains. *Proceedings of the National Academy of Sciences, USA* 95: 5857–5864.
- Sela I, Ashkenazy H, Katoh K, Pupko T. 2015. GUIDANCE2: accurate detection of unreliable alignment regions accounting for the uncertainty of multiple parameters. *Nucleic Acids Research* 43: W7–W14.
- Siao W, Wang P, Voigt B, Hussey PJ, Baluska F. 2016. Arabidopsis SYT1 maintains stability of cortical endoplasmic reticulum networks and VAP27-1-enriched endoplasmic reticulum–plasma membrane contact sites. *Journal of Experimental Botany* 67: 6161–6171.
- Soto G, Alleva K, Amodeo G, Muschietti J, Ayub ND. 2012. New insight into the evolution of aquaporins from flowering plants and vertebrates: orthologous identification and functional transfer is possible. *Gene* 503: 165–176.
- Stefano G, Renna L, Wormsbaecher C, Gamble J, Zienkiewicz K, Brandizzi F. 2018. Plant endocytosis requires the ER membrane-anchored proteins VAP27-1 and VAP27-3. *Cell Reports* 23: 2299–2307.
- Takano J, Yoshinari A, Luu D-T. 2017. Plant aquaporin trafficking. In: Chaumont F, Tyerman SD, eds. *Plant aquaporins*. Cham, Switzerland: Springer International Publishing, 47–81.
- Törnroth-Horsefield S, Wang Y, Hedfalk K, Johanson U, Karlsson M, Tajkhorshid E, Neutze R, Kjellbom P. 2006. Structural mechanism of plant aquaporin gating. *Nature* 439: 688–694.
- Tournaire-Roux C, Sutka M, Javot H, Gout E, Gerbeau P, Luu D-T, Blligny R, Maurel C. 2003. Cytosolic pH regulates root water transport during anoxic stress through gating of aquaporins. *Nature* 425: 393–397.
- Ueda M, Tsutsumi N, Fujimoto M. 2016. Salt stress induces internalization of plasma membrane aquaporin into the vacuole in *Arabidopsis thaliana*. *Biochemical and Biophysical Research Communications* 474: 742–746.
- Valm AM, Cohen S, Legant WR, Melunis J, Hershberg U, Wait E, Cohen AR, Davidson MW, Betzig E, Lippincott-Schwartz J. 2017. Applying systems-level spectral imaging and analysis to reveal the organelle interactome. *Nature* 546: 162–167.
- Van Bel M, Diels T, Vancaester E, Kreft L, Botzki A, Van de Peer Y, Coppens F, Vandepoele K. 2018. PLAZA 4.0: an integrative resource for functional, evolutionary and comparative plant genomics. *Nucleic Acids Research* 46: D1190–D1196.
- Wang P, Hawkins TJ, Richardson C, Cummins I, Deeks MJ, Sparkes I, Hawes C, Hussey PJ. 2014. The plant cytoskeleton, NET3C, and VAP27 mediate the link between the plasma membrane and endoplasmic reticulum. *Current Biology* 24: 1397–1405.
- Wang P, Hussey PJ. 2019. Plant ER–PM contact sites in endocytosis and autophagy: does the local composition of membrane phospholipid play a role? *Frontiers in Plant Science*. doi: 10.3389/fpls.2019.00023.
- Wang P, Richardson C, Hawkins TJ, Sparkes I, Hawes C, Hussey PJ. 2016. Plant VAP27 proteins: domain characterization, intracellular localization and role in plant development. *New Phytologist* 210: 1311–1326.
- Wu XN, Rodriguez CS, Pertl-Obermeyer H, Obermeyer G, Schulze WX. 2013. Sucrose-induced receptor kinase SIRK1 regulates a plasma membrane aquaporin in Arabidopsis. *Molecular & Cellular Proteomics* 12: 2856–2873.
- Yanef A, Sigaut L, Marquez M, Alleva K, Pietrasanta LI, Amodeo G. 2014. Heteromerization of PIP aquaporins affects their intrinsic permeability. *Proceedings of the National Academy of Sciences, USA* 111: 231–236.
- Zelazny E, Mieclicela U, Borst JW, Hemminga MA, Chaumont F. 2009. An N-terminal diacidic motif is required for the trafficking of maize aquaporins ZmPIP2;4 and ZmPIP2;5 to the plasma membrane. *The Plant Journal* 57: 346–355.
- Zimmermann P, Hirsch-Hoffmann M, Hennig L, Gruissem W. 2004. GENEVESTIGATOR. Arabidopsis microarray database and analysis toolbox. *Plant Physiology* 136: 2621–2632.

## Supporting Information

Additional Supporting Information may be found online in the Supporting Information section at the end of the article.

**Fig. S1** *ZmVAP27-1* does not interact with *NpPMA2*, a H<sup>+</sup>-ATPase PM resident.

**Fig. S2** MSD of VAPs is required for the interaction with *ZmPIP2;5*.

**Fig. S3** *ZmVAP27-1* colocalises with *ZmPIP2;5* in Hecthian strands.

**Fig. S4** *ZmVAP27-1* colocalises with *ZmPIP2;5* in NaCl stress-related structures.

**Fig. S5** *ZmVAP27-1* increases *Xenopus* oocyte  $P_f$  when co-expressed with *ZmPIP2;5*.

**Fig. S6** VAP27s in the maize genome.

**Fig. S7** VAP27 protein family phylogenetic tree reconstructed by maximum likelihood.

**Fig. S8** *ZmPIP2;5* mobility in the PM is restricted in comparison with *ZmLTi6A*.

**Methods S1** Mass spectrometry analysis.

**Methods S2** Fluorescence recovery after photobleaching assay.

**Table S1** Primers used in this work.

**Table S2** Mass spectrometry peptides information.

**Table S3** Potential *ZmPIP2;5* interacting proteins.

**Table S4** Proteins associated with the cytoskeleton that were pulled-down by different PIP2s.

Please note: Wiley Blackwell are not responsible for the content or functionality of any Supporting Information supplied by the authors. Any queries (other than missing material) should be directed to the *New Phytologist* Central Office.



## About *New Phytologist*

- *New Phytologist* is an electronic (online-only) journal owned by the New Phytologist Trust, a **not-for-profit organization** dedicated to the promotion of plant science, facilitating projects from symposia to free access for our Tansley reviews and Tansley insights.
- Regular papers, Letters, Research reviews, Rapid reports and both Modelling/Theory and Methods papers are encouraged. We are committed to rapid processing, from online submission through to publication 'as ready' via *Early View* – our average time to decision is <26 days. There are **no page or colour charges** and a PDF version will be provided for each article.
- The journal is available online at Wiley Online Library. Visit [www.newphytologist.com](http://www.newphytologist.com) to search the articles and register for table of contents email alerts.
- If you have any questions, do get in touch with Central Office ([np-centraloffice@lancaster.ac.uk](mailto:np-centraloffice@lancaster.ac.uk)) or, if it is more convenient, our USA Office ([np-usaoffice@lancaster.ac.uk](mailto:np-usaoffice@lancaster.ac.uk))
- For submission instructions, subscription and all the latest information visit [www.newphytologist.com](http://www.newphytologist.com)